

1 Submitted to *Neural Computation*

2 Direct Learning of Sparse Changes in
3 Markov Networks by Density Ratio Estimation*

4 Song Liu

song@sg.cs.titech.ac.jp

Tokyo Institute of Technology,
2-12-1 O-okayama, Meguro, Tokyo 152-8552, Japan.

<http://sugiyama-www.cs.titech.ac.jp/~song/>

John A. Quinn

jquinn@cit.ac.ug

Makerere University, P.O. Box 7062, Kampala, Uganda.

Michael U. Gutmann

michael.gutmann@helsinki.fi

University of Helsinki, Finland, P.O. Box 68, FI-00014, Finland.

Taiji Suzuki

suzuki.t.ct@m.titech.ac.jp

Tokyo Institute of Technology,
2-12-1 O-okayama, Meguro, Tokyo 152-8552, Japan.

Masashi Sugiyama

sugi@cs.titech.ac.jp

Tokyo Institute of Technology,
2-12-1 O-okayama, Meguro, Tokyo 152-8552, Japan.

<http://sugiyama-www.cs.titech.ac.jp/>

5 **Abstract**

6 We propose a new method for detecting changes in Markov network structure
7 between two sets of samples. Instead of naively fitting two Markov network models
8 separately to the two data sets and figuring out their difference, we *directly* learn the
9 network structure change by estimating the ratio of Markov network models. This
10 density-ratio formulation naturally allows us to introduce sparsity in the network
11 structure change, which highly contributes to enhancing interpretability. Further-
12 more, computation of the normalization term, which is a critical bottleneck of the
13 naive approach, can be remarkably mitigated. We also give the dual formulation
14 of the optimization problem, which further reduces the computation cost for large-
15 scale Markov networks. Through experiments, we demonstrate the usefulness of our
16 method.

*An earlier version of this work was presented at European Conference on Machine Learning and Principles and Practice of Knowledge Discovery in Databases (ECML/PKDD2013) on Sep. 23-27, 2013.

1 Introduction

Changes in interactions between random variables are interesting in many real-world phenomena. For example, genes may interact with each other in different ways when external stimuli change, co-occurrence between words may disappear/appear when the domains of text corpora shift, and correlation among pixels may change when a surveillance camera captures anomalous activities. Discovering such changes in interactions is a task of great interest in machine learning and data mining, because it provides useful insights into underlying mechanisms in many real-world applications.

In this paper, we consider the problem of detecting changes in conditional independence among random variables between two sets of data. Such conditional independence structure can be expressed via an undirected graphical model called a *Markov network* (MN) (Bishop, 2006; Wainwright and Jordan, 2008; Koller and Friedman, 2009), where nodes and edges represent variables and their conditional dependencies. As a simple and widely applicable case, the 2nd-order pairwise MN model has been thoroughly studied recently (Ravikumar et al., 2010; Lee et al., 2007). Following this line, we also focus on the pairwise MN model as a representative example.

A naive approach to change detection in MNs is the two-step procedure of first estimating two MNs separately from two sets of data by *maximum likelihood estimation* (MLE), and then comparing the structure of the learned MNs. However, MLE is often computationally intractable due to the normalization factor included in the density model. Although there are estimation methods which do not rely on knowing the normalization factor (Gelman, 1995; Hinton, 2002; Hyvärinen, 2005; Gutmann and Hyvärinen, 2012), Gaussianity is often assumed in practice for computing the normalization factor analytically (Hastie et al., 2001). However, this Gaussian assumption is highly restrictive in practice.

Another conceptual weakness of the above two-step procedure is that structure change is not directly learned. This indirect nature causes a problem, for example, if we want to learn a sparse structure change. For learning sparse changes, we may utilize ℓ_1 -regularized MLE (Banerjee et al., 2008; Friedman et al., 2008; Lee et al., 2007), which produces sparse MNs and thus the change between MNs also becomes sparse. However, this approach does not work if each MN is dense but only change is sparse.

To mitigate this indirect nature, the *fused-lasso* (Tibshirani et al., 2005) is useful, where two MNs are simultaneously learned with a sparsity-inducing penalty on the *difference* between two MN parameters (Zhang and Wang, 2010). Although this fused-lasso approach allows us to learn sparse structure change naturally, the restrictive Gaussian assumption is still necessary to obtain the solution in a computationally tractable way.

A *nonparanormal* assumption (Liu et al., 2009, 2012) is a useful generalization of the Gaussian assumption. A nonparanormal distribution is a *semi-parametric Gaussian copula* where each Gaussian variable is transformed by a monotone non-linear function. Nonparanormal distributions are much more flexible than Gaussian distributions thanks to the feature-wise non-linear transformation, while the normalization factors can still be computed analytically. Thus, the fused-lasso method combined with nonparanormal

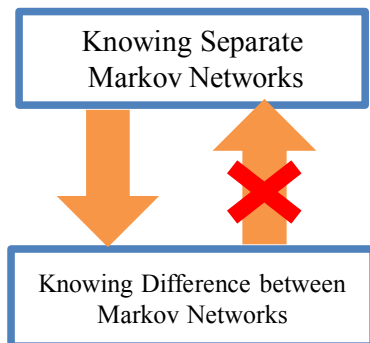


Figure 1: The rationale of direct structural change learning: finding the difference between two MNs is a more specific task than finding the entire structures of those two networks, and hence should be possible to learn with less data.

59 models would be one of the state-of-the-art approaches to change detection in MNs.
 60 However, the fused-lasso method is still based on separate modeling of two MNs, and its
 61 computation for more general non-Gaussian distributions is challenging.

62 For handling intractable integrals in normalization terms, another approach can be
 63 considered. By introducing an *instrumental distribution*, the intractable integrals can
 64 be approximated by *importance sampling* (Robert and Casella, 2005), and thus the so-
 65 lution of non-Gaussian MLE can be obtained. However, an inappropriate choice of the
 66 instrumental distribution may lead to an estimator with high variance (Wasserman, 2010;
 67 Robert and Casella, 2005). Moreover, a two-step procedure is still required for change
 68 detection.

69 In this paper, we propose a more direct approach to structural change learning in MNs
 70 based on *density ratio estimation* (DRE) (Sugiyama et al., 2012). Our method does not
 71 separately model two MNs, but directly models the *change* in two MNs. This idea follows
 72 Vapnik’s principle (Vapnik, 1998):

73 If you possess a restricted amount of information for solving some problem,
 74 try to solve the problem directly and never solve a more general problem as
 75 an intermediate step. It is possible that the available information is sufficient
 76 for a direct solution but is insufficient for solving a more general intermediate
 77 problem.

78 This principle was used in the development of *support vector machines* (SVMs): rather
 79 than modeling two classes of samples, SVM directly learns a decision boundary that is
 80 sufficient for performing pattern recognition. In the current context, estimating two MNs
 81 is more general than detecting changes in MNs (Figure 1). By directly detecting changes
 82 in MNs, we can also halve the number of parameters, from two MNs to one MN-difference.

83 Furthermore, the normalization factor in our DRE-based method can be approximated
 84 efficiently, because the normalization term in a density ratio function takes the form of
 85 the expectation over a data distribution and thus it can be simply approximated by the

86 sample average without additional sampling. Through experiments on gene expression
 87 and Twitter data analysis, we demonstrate the usefulness of our proposed approach. In
 88 this paper, only the pairwise MN is considered. The generalization to higher-order MNs
 89 is straightforward in theory but may be challenging in computation.

90 The remainder of this paper is structured as follows. In Section 2, we formulate the
 91 problem of detecting structural changes and review currently available approaches. We
 92 then propose our DRE-based structural change detection method in Section 3. Results
 93 of illustrative and real-world experiments are reported in Section 4 and Section 5, respec-
 94 tively. Finally, we conclude our work and show the future direction in Section 6.

95 2 Problem Formulation and Related Methods

96 In this section, we formulate the problem of change detection in Markov network structure
 97 and review existing approaches.

98 2.1 Problem Formulation

Consider two sets of independent samples drawn separately from two probability distri-
 butions P and Q on \mathbb{R}^d :

$$\{\mathbf{x}_i^P\}_{i=1}^{n_P} \stackrel{\text{i.i.d.}}{\sim} P \text{ and } \{\mathbf{x}_i^Q\}_{i=1}^{n_Q} \stackrel{\text{i.i.d.}}{\sim} Q.$$

We assume that P and Q belong to the family of *Markov networks* (MNs) consisting of
 univariate and bivariate factors¹, i.e., their respective probability densities p and q are
 expressed as

$$p(\mathbf{x}; \boldsymbol{\theta}) = \frac{1}{Z(\boldsymbol{\theta})} \exp \left(\sum_{u,v=1, u \geq v}^d \boldsymbol{\theta}_{u,v}^\top \mathbf{f}(x^{(u)}, x^{(v)}) \right), \quad (1)$$

where $\mathbf{x} = (x^{(1)}, \dots, x^{(d)})^\top$, $\boldsymbol{\theta}_{u,v}$ are parameters, and

$$\boldsymbol{\theta} = (\boldsymbol{\theta}_{1,1}^\top, \dots, \boldsymbol{\theta}_{d,1}^\top, \boldsymbol{\theta}_{2,2}^\top, \dots, \boldsymbol{\theta}_{d,2}^\top, \dots, \boldsymbol{\theta}_{d,d}^\top)^\top.$$

$\mathbf{f}(x^{(u)}, x^{(v)})$ are bivariate vector-valued basis functions. $Z(\boldsymbol{\theta})$ is the normalization factor

$$Z(\boldsymbol{\theta}) = \int \exp \left(\sum_{u,v=1, u \geq v}^d \boldsymbol{\theta}_{u,v}^\top \mathbf{f}(x^{(u)}, x^{(v)}) \right) d\mathbf{x}.$$

99 $q(\mathbf{x}; \boldsymbol{\theta})$ is defined in the same way.

100 Our goal is to detect the change in conditional independence between random variables
 101 $x^{(1)}, \dots, x^{(d)}$ from P to Q .

¹ Note that the proposed algorithm itself can be applied to *any* MNs containing higher-order factors.

2.2 Sparse MLE and Graphical Lasso (Glasso)

Maximum likelihood estimation (MLE) with group ℓ_1 -regularization has been widely used for estimating the sparse structure of MNs (Schmidt and Murphy, 2010; Ravikumar et al., 2010; Lee et al., 2007):

$$\max_{\boldsymbol{\theta}} \left[\frac{1}{n_P} \sum_{i=1}^{n_P} \log p(\mathbf{x}_i^P; \boldsymbol{\theta}) - \lambda \sum_{u,v=1, u \geq v}^d \|\boldsymbol{\theta}_{u,v}\| \right], \quad (2)$$

where $\|\cdot\|$ denotes the ℓ_2 -norm. As λ increases, $\|\boldsymbol{\theta}_{u,v}\|$ may drop to 0. Thus, this method favors an MN that encodes more conditional independencies among variables. For computing the normalization term $Z(\boldsymbol{\theta})$ in Eq.(1), sampling techniques such as Markov-chain Monte-Carlo are usually employed. However, obtaining a reasonable approximate by such sampling methods becomes computationally more difficult as the dimension d grows.

To avoid this computational problem, the Gaussian assumption is often imposed (Friedman et al., 2008; Meinshausen and Bühlmann, 2006). If we consider a zero-mean Gaussian distribution, the following $p(\mathbf{x}; \boldsymbol{\Theta})$ can be used to replace the density model in Eq.(2):

$$p(\mathbf{x}; \boldsymbol{\Theta}) = \frac{\det(\boldsymbol{\Theta})^{1/2}}{(2\pi)^{d/2}} \exp\left(-\frac{1}{2} \mathbf{x}^\top \boldsymbol{\Theta} \mathbf{x}\right),$$

where $\boldsymbol{\Theta}$ is the inverse covariance matrix (a.k.a. the precision matrix) and $\det(\cdot)$ denotes the determinant. Then $\boldsymbol{\Theta}$ is learned by

$$\max_{\boldsymbol{\Theta}} \left[\log \det(\boldsymbol{\Theta}) - \text{tr}(\boldsymbol{\Theta} \mathbf{S}^P) - \lambda \|\boldsymbol{\Theta}\|_1 \right],$$

where \mathbf{S}^P is the sample covariance matrix of $\{\mathbf{x}_i^P\}_{i=1}^n$. $\|\boldsymbol{\Theta}\|_1$ is the ℓ_1 -norm of $\boldsymbol{\Theta}$, i.e., the absolute sum of all elements. This formulation has been studied intensively in Banerjee et al. (2008), and a computationally efficient algorithm called the *graphical lasso* has been proposed (Friedman et al., 2008).

Sparse changes in conditional independence structure between P and Q can be detected by comparing two MNs separately estimated using sparse MLE. However, this approach implicitly assumes that two MNs are sparse, which is not necessarily true even if the change is sparse.

2.3 Fused-Lasso (Flasso) Method

To more naturally handle sparse changes in conditional independence structure between P and Q , a method based on *fused-lasso* (Tibshirani et al., 2005) has been developed (Zhang and Wang, 2010), which directly sparsifies the *difference* between parameters.

The original method conducts *feature-wise neighbourhood regression* (Meinshausen and Bühlmann, 2006) jointly for P and Q , which can be conceptually understood as maximizing the local conditional Gaussian likelihood jointly on each

feature (Ravikumar et al., 2010). Thus, a slightly more general form of the learning criterion may be summarized as

$$\max_{\boldsymbol{\theta}_s^P, \boldsymbol{\theta}_s^Q} [\ell_s^P(\boldsymbol{\theta}_s^P) + \ell_s^Q(\boldsymbol{\theta}_s^Q) - \lambda_1(\|\boldsymbol{\theta}_s^P\|_1 + \|\boldsymbol{\theta}_s^Q\|_1) - \lambda_2\|\boldsymbol{\theta}_s^P - \boldsymbol{\theta}_s^Q\|_1],$$

where $\ell_s^P(\boldsymbol{\theta})$ is the log conditional likelihood for the s -th element $x^{(s)} \in \mathbb{R}$ given the rest $\mathbf{x}^{(-s)} \in \mathbb{R}^{d-1}$:

$$\ell_s^P(\boldsymbol{\theta}) = \frac{1}{n_P} \sum_{i=1}^{n_P} \log p(x_i^{(s)P} | \mathbf{x}_i^{(-s)P}; \boldsymbol{\theta}).$$

121 $\ell_s^Q(\boldsymbol{\theta})$ is defined in the same way as $\ell_s^P(\boldsymbol{\theta})$. However, considering general continuous
 122 distribution for $\ell_s^P(\boldsymbol{\theta})$ or $\ell_s^Q(\boldsymbol{\theta})$ is still difficult, because of the normalization issue described
 123 in Section 2.2.

124 2.4 Nonparanormal (NPN) Extensions

125 In the above methods, Gaussianity is required in practice to compute the normalization
 126 factor efficiently, which is a highly restrictive assumption.

127 To overcome this restriction, it has become popular to perform structure learning under
 128 the *nonparanormal* settings (Liu et al., 2009, 2012), where the Gaussian distribution is
 129 replaced by a *semi-parametric Gaussian copula*. $\mathbf{x} = (x^{(1)}, \dots, x^{(d)})^\top$ is said to follow a
 130 *nonparanormal* distribution, if there exists a set of monotone and differentiable functions,
 131 $\{h_i(x)\}_{i=1}^d$, such that $\mathbf{h}(\mathbf{x}) = (h_1(x^{(1)}), \dots, h_d(x^{(d)}))^\top$ follows the Gaussian distribution.
 132 Nonparanormal distributions are much more flexible than Gaussian distributions thanks
 133 to the non-linear transformation $\{h_i(x)\}_{i=1}^d$, while the normalization factors can still be
 134 computed in an analytical way.

135 2.5 Importance-Sampling MLE (IS-Glasso)

136 Another way to obtain the MLE solution under non-Gaussian distributions is *importance*
 137 *sampling*.

Suppose we try to maximize the log-likelihood²,

$$\begin{aligned} \ell_{\text{MLE}}(\boldsymbol{\theta}) &= \frac{1}{n_P} \sum_{i=1}^{n_P} \log p(\mathbf{x}_i^P; \boldsymbol{\theta}) \\ &= \frac{1}{n_P} \sum_{i=1}^{n_P} \sum_{u \geq v} \boldsymbol{\theta}_{u,v}^\top \mathbf{f}(x_i^{(u)P}, x_i^{(v)P}) - \log \int \exp \left(\sum_{u \geq v} \boldsymbol{\theta}_{u,v}^\top \mathbf{f}(x^{(u)}, x^{(v)}) \right) d\mathbf{x}. \end{aligned} \quad (3)$$

The key idea of importance sampling is to compute the integral by the expectation over an easy-to-sample instrumental density $p'(\mathbf{x})$ (e.g., Gaussian) weighted according to

²From now on, we simplify $\sum_{u,v=1, u \geq v}^d$ as $\sum_{u \geq v}$.

the *importance* $1/p'(\mathbf{x})$. More specifically, using i.i.d. samples $\{\mathbf{x}'_i\}_{i=1}^{n'} \stackrel{\text{i.i.d.}}{\sim} p'(\mathbf{x})$, the last term of Eq.(3) can be approximately computed as follows:

$$\begin{aligned} \log \int \exp \left(\sum_{u \geq v} \boldsymbol{\theta}_{u,v}^\top \mathbf{f}(x^{(u)}, x^{(v)}) \right) d\mathbf{x} &= \log \int p'(\mathbf{x}) \frac{\exp \left(\sum_{u \geq v} \boldsymbol{\theta}_{u,v}^\top \mathbf{f}(x^{(u)}, x^{(v)}) \right)}{p'(\mathbf{x})} d\mathbf{x} \\ &\approx \log \frac{1}{n'} \sum_{i=1}^{n'} \frac{\exp \left(\sum_{u \geq v} \boldsymbol{\theta}_{u,v}^\top \mathbf{f}(x'_i{}^{(u)}, x'_i{}^{(v)}) \right)}{p'(\mathbf{x}'_i)}, \end{aligned}$$

138 Importance sampling tends to produce an estimate with large variance if the instru-
139 mental distribution is not carefully chosen. Although it is often suggested to use a density
140 whose shape is similar to the function to be integrated but with thicker tails as p' , it is
141 not straightforward in practice to decide which p' to choose, especially when the dimen-
142 sionality of \mathbf{x} is high (Wasserman, 2010).

We can also consider an importance-sampling version of the Flasso method (which we call IS-Flasso)³

$$\max_{\boldsymbol{\theta}^P, \boldsymbol{\theta}^Q} \left[\ell_{\text{MLE}}^P(\boldsymbol{\theta}^P) + \ell_{\text{MLE}}^Q(\boldsymbol{\theta}^Q) - \lambda_1 (\|\boldsymbol{\theta}^P\|^2 + \|\boldsymbol{\theta}^Q\|^2) - \lambda_2 \sum_{u \geq v} \|\boldsymbol{\theta}_{u,v}^P - \boldsymbol{\theta}_{u,v}^Q\| \right],$$

143 where both $\ell_{\text{MLE}}^P(\boldsymbol{\theta}^P)$ and $\ell_{\text{MLE}}^Q(\boldsymbol{\theta}^Q)$ are approximated by importance sampling for non-
144 Gaussian distributions. However, in the same way as IS-Glasso, the choice of the instru-
145 mental distribution is difficult.

146 3 Direct Learning of Structural Changes via Density 147 Ratio Estimation

148 The fused-lasso method can more naturally handle sparse changes in MNs than separate
149 sparse MLE. However, the fused-lasso method is still based on separate modeling of two
150 MNs, and its computation for general high-dimensional non-Gaussian distributions is
151 challenging.

152 In this section, we propose to directly learn structural changes based on *density ratio*
153 *estimation* (Sugiyama et al., 2012). Our approach does not involve separate modeling of
154 each MN and allows us to approximate the normalization term efficiently.

155 3.1 Density Ratio Formulation for Structural Change Detection

156 Our key idea is to consider the ratio of p and q :

³For implementation simplicity, we maximize the joint likelihood of p and q , instead of its feature-wise conditional likelihood. We also switch the first penalty term from ℓ_1 to ℓ_2 . Since sparse $\boldsymbol{\theta}$ does not lead to a sparse MN if the size of $\boldsymbol{\theta}_{u,v}$ is larger than 1, ℓ_2 would be a natural choice if the identifiability is the main concern of introducing this term.

$$\frac{p(\mathbf{x}; \boldsymbol{\theta}^P)}{q(\mathbf{x}; \boldsymbol{\theta}^Q)} \propto \exp \left(\sum_{u \geq v} (\boldsymbol{\theta}_{u,v}^P - \boldsymbol{\theta}_{u,v}^Q)^\top \mathbf{f}(x^{(u)}, x^{(v)}) \right).$$

157 Here $\boldsymbol{\theta}_{u,v}^P - \boldsymbol{\theta}_{u,v}^Q$ encodes the difference between P and Q for factor $\mathbf{f}(x^{(u)}, x^{(v)})$, i.e.,
 158 $\boldsymbol{\theta}_{u,v}^P - \boldsymbol{\theta}_{u,v}^Q$ is zero if there is no change in the factor $\mathbf{f}(x^{(u)}, x^{(v)})$.

Once we consider the ratio of p and q , we actually do not have to estimate $\boldsymbol{\theta}_{u,v}^P$ and $\boldsymbol{\theta}_{u,v}^Q$; instead estimating their difference $\boldsymbol{\theta}_{u,v} = \boldsymbol{\theta}_{u,v}^P - \boldsymbol{\theta}_{u,v}^Q$ is sufficient for change detection:

$$r(\mathbf{x}; \boldsymbol{\theta}) = \frac{1}{N(\boldsymbol{\theta})} \exp \left(\sum_{u \geq v} \boldsymbol{\theta}_{u,v}^\top \mathbf{f}(x^{(u)}, x^{(v)}) \right), \quad (4)$$

where

$$N(\boldsymbol{\theta}) = \int q(\mathbf{x}) \exp \left(\sum_{u \geq v} \boldsymbol{\theta}_{u,v}^\top \mathbf{f}(x^{(u)}, x^{(v)}) \right) d\mathbf{x}.$$

The normalization term $N(\boldsymbol{\theta})$ guarantees⁴

$$\int q(\mathbf{x}) r(\mathbf{x}; \boldsymbol{\theta}) d\mathbf{x} = 1.$$

159 Thus, in this density ratio formulation, we are no longer modeling p and q separately,
 160 but we model the change from p to q *directly*. This direct nature would be more suitable
 161 for change detection purposes according to Vapnik's principle that encourages avoidance
 162 of solving more general problems as an intermediate step (Vapnik, 1998). This direct
 163 formulation also allows us to halve the number of parameters from both $\boldsymbol{\theta}^P$ and $\boldsymbol{\theta}^Q$ to
 164 only $\boldsymbol{\theta}$.

⁴ If the model $q(\mathbf{x}; \boldsymbol{\theta}^Q)$ is correctly specified, i.e., there exists $\boldsymbol{\theta}^{Q*}$ such that $q(\mathbf{x}; \boldsymbol{\theta}^{Q*}) = q(\mathbf{x})$, then $N(\boldsymbol{\theta})$ can be interpreted as importance sampling of $Z(\boldsymbol{\theta}^P)$ via instrumental distribution $q(\mathbf{x})$. Since

$$Z(\boldsymbol{\theta}^P) = \int q(\mathbf{x}) \frac{\exp \left(\sum_{u \geq v} \boldsymbol{\theta}_{u,v}^P \cdot \mathbf{f}(x^{(u)}, x^{(v)}) \right)}{q(\mathbf{x}; \boldsymbol{\theta}^{Q*})} d\mathbf{x},$$

where $q(\mathbf{x}; \boldsymbol{\theta}^{Q*}) = q(\mathbf{x})$, we have

$$N(\boldsymbol{\theta}^P - \boldsymbol{\theta}^{Q*}) = \frac{Z(\boldsymbol{\theta}^P)}{Z(\boldsymbol{\theta}^{Q*})} = \int q(\mathbf{x}) \exp \left(\sum_{u \geq v} (\boldsymbol{\theta}_{u,v}^P - \boldsymbol{\theta}_{u,v}^{Q*})^\top \mathbf{f}(x^{(u)}, x^{(v)}) \right) d\mathbf{x}.$$

This is exactly the normalization term of the ratio $p(\mathbf{x}; \boldsymbol{\theta}^P)/q(\mathbf{x}; \boldsymbol{\theta}^{Q*})$. However, we note that the density ratio estimation method we use in this paper is consistent to the optimal solution in the model even without the correct model assumption (Sugiyama et al., 2008). An alternative normalization term $N'(\boldsymbol{\theta}, \boldsymbol{\theta}^Q) = \int q(\mathbf{x}; \boldsymbol{\theta}^Q) r(\mathbf{x}; \boldsymbol{\theta}) d\mathbf{x}$ may also be considered, as in the case of MLE. However, this alternative form requires an extra parameter $\boldsymbol{\theta}^Q$ which is not our main interest.

Furthermore, the normalization factor $N(\boldsymbol{\theta})$ in the density ratio formulation can be easily approximated by the sample average over $\{\mathbf{x}_i^{(Q)}\}_{i=1}^{n_Q} \stackrel{\text{i.i.d.}}{\sim} q(\mathbf{x})$, because $N(\boldsymbol{\theta})$ is the expectation over $q(\mathbf{x})$:

$$N(\boldsymbol{\theta}) \approx \frac{1}{n_Q} \sum_{i=1}^{n_Q} \exp \left(\sum_{u \geq v} \boldsymbol{\theta}_{u,v}^\top \mathbf{f}(x_i^{(u)Q}, x_i^{(v)Q}) \right).$$

165 3.2 Direct Density-Ratio Estimation

166 Density ratio estimation has been recently introduced to the machine learning community
 167 and is proven to be useful in a wide range of applications (Sugiyama et al., 2012). Here,
 168 we concentrate on the density ratio estimator called the *Kullback-Leibler importance es-*
 169 *timation procedure* (KLIEP) for a log-linear model (Sugiyama et al., 2008; Tsuboi et al.,
 170 2009).

For a density ratio model $r(\mathbf{x}; \boldsymbol{\theta})$, the KLIEP method minimizes the Kullback-Leibler divergence from $p(\mathbf{x})$ to $\hat{p}(\mathbf{x}) = q(\mathbf{x})r(\mathbf{x}; \boldsymbol{\theta})$:

$$\begin{aligned} \text{KL}[p \parallel \hat{p}] &= \int p(\mathbf{x}) \log \frac{p(\mathbf{x})}{q(\mathbf{x})r(\mathbf{x}; \boldsymbol{\theta})} d\mathbf{x} \\ &= \text{Const.} - \int p(\mathbf{x}) \log r(\mathbf{x}; \boldsymbol{\theta}) d\mathbf{x}. \end{aligned} \quad (5)$$

Note that our density-ratio model (4) automatically satisfies the non-negativity and normalization constraints:

$$r(\mathbf{x}; \boldsymbol{\theta}) \geq 0 \quad \text{and} \quad \int q(\mathbf{x})r(\mathbf{x}; \boldsymbol{\theta}) d\mathbf{x} = 1.$$

In practice, we maximize the empirical approximation of the second term in Eq.(5):

$$\begin{aligned} \ell_{\text{KLIEP}}(\boldsymbol{\theta}) &= \frac{1}{n_P} \sum_{i=1}^{n_P} \log r(\mathbf{x}_i^P; \boldsymbol{\theta}) \\ &= \frac{1}{n_P} \sum_{i=1}^{n_P} \sum_{u \geq v} \boldsymbol{\theta}_{u,v}^\top \mathbf{f}(x_i^{(u)P}, x_i^{(v)P}) \\ &\quad - \log \left(\frac{1}{n_Q} \sum_{i=1}^{n_Q} \exp \left(\sum_{u \geq v} \boldsymbol{\theta}_{u,v}^\top \mathbf{f}(x_i^{(u)Q}, x_i^{(v)Q}) \right) \right). \end{aligned}$$

Because $\ell_{\text{KLIEP}}(\boldsymbol{\theta})$ is concave with respect to $\boldsymbol{\theta}$, its global maximizer can be numerically found by standard optimization techniques such as gradient ascent or quasi-Newton

methods. The gradient of ℓ_{KLIEP} with respect to $\boldsymbol{\theta}_{u,v}$ is given by

$$\begin{aligned} \nabla_{\boldsymbol{\theta}_{u,v}} \ell_{\text{KLIEP}}(\boldsymbol{\theta}) &= \frac{1}{n_P} \sum_{i=1}^{n_P} \mathbf{g}(\mathbf{x}_i^{(u)P}, \mathbf{x}_i^{(v)P}) \\ &\quad - \frac{\frac{1}{n_Q} \sum_{i=1}^{n_Q} \exp\left(\sum_{u' \geq v'} \boldsymbol{\theta}_{u',v'}^\top \mathbf{f}(x_i^{(u')Q}, x_i^{(v')Q})\right) \mathbf{f}(x_i^{(u)Q}, x_i^{(v)Q})}{\frac{1}{n_Q} \sum_{j=1}^{n_Q} \exp\left(\sum_{u'' \geq v''} \boldsymbol{\theta}_{u'',v''}^\top \mathbf{f}(x_j^{(u'')Q}, x_j^{(v'')Q})\right)}, \end{aligned}$$

171 which can be computed in a straightforward manner for *any* feature vector $\mathbf{f}(x^{(u)}, x^{(v)})$.

172 3.3 Sparsity-Inducing Norm

173 To find a sparse change between P and Q , we propose to regularize our KLIEP solution
 174 with a sparsity-inducing norm $\sum_{u \geq v} \|\boldsymbol{\theta}_{u,v}\|$. Note that the MLE approach sparsifies both
 175 $\boldsymbol{\theta}^P$ and $\boldsymbol{\theta}^Q$ so that the difference $\boldsymbol{\theta}^P - \boldsymbol{\theta}^Q$ is also sparsified. On the other hand, we directly
 176 sparsify the difference $\boldsymbol{\theta}^P - \boldsymbol{\theta}^Q$; thus our method can still work well even if $\boldsymbol{\theta}^P$ and $\boldsymbol{\theta}^Q$
 177 are dense.

In practice, we may use the following *elastic-net* penalty (Zou and Hastie, 2005) to better control overfitting to noisy data:

$$\max_{\boldsymbol{\theta}} \left[\ell_{\text{KLIEP}}(\boldsymbol{\theta}) - \lambda_1 \|\boldsymbol{\theta}\|^2 - \lambda_2 \sum_{u \geq v} \|\boldsymbol{\theta}_{u,v}\| \right], \quad (6)$$

178 where $\|\boldsymbol{\theta}\|^2$ penalizes the magnitude of the entire parameter vector.

179 3.4 Dual Formulation for High-Dimensional Data

180 The solution of the optimization problem (6) can be easily obtained by standard sparse
 181 optimization methods. However, in the case where the input dimensionality d is high
 182 (which is often the case in our setup), the dimensionality of parameter vector $\boldsymbol{\theta}$ is large,
 183 and thus obtaining the solution can be computationally expensive. Here, we derive a dual
 184 optimization problem (Boyd and Vandenberghe, 2004) for the proposed method, which
 185 can be solved more efficiently when $\boldsymbol{\theta}$ is high-dimensional (Figure 2).

First, we rewrite the optimization problem (6) as

$$\begin{aligned} \min_{\boldsymbol{\theta}, \mathbf{w}} \left[\log \left(\sum_{i=1}^{n_Q} \exp(w_i) \right) - \boldsymbol{\theta}^\top \mathbf{g} + \frac{\lambda_1}{2} \boldsymbol{\theta}^\top \boldsymbol{\theta} + \lambda_2 \sum_{u \geq v} \|\boldsymbol{\theta}_{u,v}\| - C \right] \quad (7) \\ \text{subject to } \mathbf{w} = \mathbf{H}^\top \boldsymbol{\theta}, \end{aligned}$$

where

$$\begin{aligned} \mathbf{H} &= (\mathbf{H}_{1,1}^\top, \dots, \mathbf{H}_{d,1}^\top, \mathbf{H}_{2,2}^\top, \dots, \mathbf{H}_{d,2}^\top, \dots, \mathbf{H}_{d,d}^\top)^\top, \\ \mathbf{H}_{u,v} &= [\mathbf{f}(x_1^{(u)Q}, x_1^{(v)Q}), \dots, \mathbf{f}(x_{n_Q}^{(u)Q}, x_{n_Q}^{(v)Q})], \\ \mathbf{g} &= (\mathbf{g}_{1,1}^\top, \dots, \mathbf{g}_{d,1}^\top, \mathbf{g}_{2,2}^\top, \dots, \mathbf{g}_{d,2}^\top, \dots, \mathbf{g}_{d,d}^\top)^\top, \quad \mathbf{g}_{u,v} = \frac{1}{n_P} \sum_{i=1}^{n_P} \mathbf{f}(x_i^{(u)P}, x_i^{(v)P}), \\ C &= \log n_Q, \quad \mathbf{w} = (w_1, \dots, w_{n_Q})^\top. \end{aligned}$$

With Lagrange multipliers $\boldsymbol{\alpha} = (\alpha_1, \dots, \alpha_{n_Q})^\top$, the Lagrangian of (7) is

$$\begin{aligned} \mathcal{L}(\boldsymbol{\alpha}) &= \min_{\mathbf{w}, \boldsymbol{\theta}} \left[\log \sum_{i=1}^{n_Q} \exp(w_i) - \boldsymbol{\theta}^\top \mathbf{g} + \frac{\lambda_1}{2} \boldsymbol{\theta}^\top \boldsymbol{\theta} + \lambda_2 \sum_{u \geq v} \|\boldsymbol{\theta}_{u,v}\| - (\mathbf{w} - \mathbf{H}^\top \boldsymbol{\theta})^\top \boldsymbol{\alpha} \right] - C \\ &= \min_{\mathbf{w}} \left[\log \sum_{i=1}^{n_Q} \exp(w_i) - \mathbf{w}^\top \boldsymbol{\alpha} \right] \\ &\quad + \min_{\boldsymbol{\theta}} \left[\boldsymbol{\theta}^\top (\mathbf{H} \boldsymbol{\alpha} - \mathbf{g}) + \frac{\lambda_1}{2} \boldsymbol{\theta}^\top \boldsymbol{\theta} + \lambda_2 \sum_{u \geq v} \|\boldsymbol{\theta}_{u,v}\| \right] - C \\ &= \min_{\mathbf{w}} \psi_1(\mathbf{w}) + \min_{\boldsymbol{\theta}} \psi_2(\boldsymbol{\theta}) - C. \end{aligned} \tag{8}$$

A few lines of algebra can show that $\psi_1(\mathbf{w})$ reaches the minimum $-\sum_{i=1}^{n_Q} \alpha_i \log \alpha_i$ at

$$\alpha_i = \frac{\exp(w_i)}{\sum_{i=1}^{n_Q} \exp(w_i)}, \quad i = 1, \dots, n_Q.$$

Note that extra constraints are implied from the above equation:

$$\alpha_1, \dots, \alpha_{n_Q} \geq 0 \text{ and } \sum_{i=1}^{n_Q} \alpha_i = 1.$$

Since $\psi_2(\boldsymbol{\theta})$ is not differentiable at $\boldsymbol{\theta}_{u,v} = \mathbf{0}$, we can only obtain its subgradient:

$$\nabla_{\boldsymbol{\theta}_{u,v}} \psi_2(\boldsymbol{\theta}) = -\mathbf{m}_{u,v} + \lambda_1 \boldsymbol{\theta} + \lambda_2 \nabla_{\boldsymbol{\theta}_{u,v}} \|\boldsymbol{\theta}_{u,v}\|,$$

where

$$\begin{aligned} \mathbf{m}_{u,v} &= \mathbf{g}_{u,v} - \mathbf{H}_{u,v} \boldsymbol{\alpha}, \\ \nabla_{\boldsymbol{\theta}_{u,v}} \|\boldsymbol{\theta}_{u,v}\| &= \begin{cases} \frac{\boldsymbol{\theta}_{u,v}}{\|\boldsymbol{\theta}_{u,v}\|} & \text{if } \boldsymbol{\theta}_{u,v} \neq \mathbf{0}, \\ \{\mathbf{y} \mid \|\mathbf{y}\| \leq 1\} & \text{if } \boldsymbol{\theta}_{u,v} = \mathbf{0}. \end{cases} \end{aligned}$$

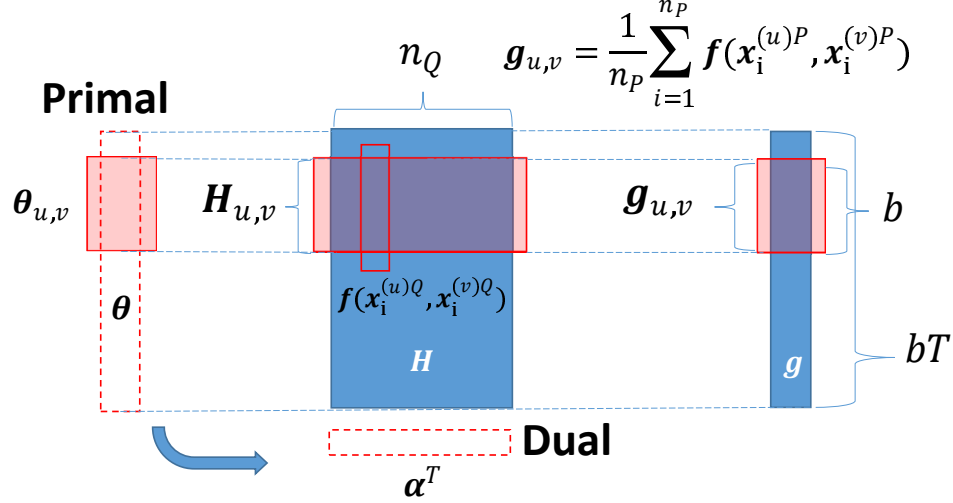


Figure 2: Schematics of primal and dual objectives. b denotes the number of basis functions and T denotes the number of factors. Because we are considering pairwise factors, $T = \mathcal{O}(d^2)$ for input dimensionality d .

By setting $\nabla_{\theta_t} \psi_2(\theta) = \mathbf{0}$, we can obtain the solution to this minimization problem as

$$\theta_t = \begin{cases} \left(\frac{1}{\lambda_1} - \frac{\lambda_2}{\lambda_1 \|\mathbf{m}_{u,v}\|} \right) \mathbf{m}_{u,v} & \text{if } \|\mathbf{m}_{u,v}\| > \lambda_2, \\ \mathbf{0} & \text{if } \|\mathbf{m}_{u,v}\| \leq \lambda_2. \end{cases} \quad (9)$$

Substituting the solutions of the above two minimization problems with respect to θ and \mathbf{w} into (8), we obtain the dual optimization problem:

$$\begin{aligned} \max_{\boldsymbol{\alpha} = (\alpha_1, \dots, \alpha_{n_Q})^\top} & - \sum_{i=1}^{n_Q} \alpha_i \log \alpha_i - \sum_{u \geq v} \xi_{u,v}(\boldsymbol{\alpha}) - C \\ \text{subject to } & \alpha_1, \dots, \alpha_{n_Q} \geq 0 \text{ and } \sum_{i=1}^{n_Q} \alpha_i = 1, \end{aligned} \quad (10)$$

where

$$\xi_{u,v}(\boldsymbol{\alpha}) = \begin{cases} \frac{\|\mathbf{m}_{u,v}\|^2 - \lambda_2^2}{2\lambda_1} - \frac{\lambda_2 \|\mathbf{m}_{u,v}\| - \lambda_2^2}{\lambda_1} & \text{if } \|\mathbf{m}_{u,v}\| > \lambda_2, \\ 0 & \text{if } \|\mathbf{m}_{u,v}\| \leq \lambda_2. \end{cases}$$

186 Note that the dimensionality of the dual variable $\boldsymbol{\alpha}$ is equal to n_Q , while that of θ is
 187 quadratic with respect to the input dimensionality d because we are considering pairwise
 188 factors. Thus, if d is not small and n_Q is not very large (which is often the case in

our experiments shown later), solving the dual problem would be computationally more efficient. Furthermore, the dual objective (or its gradient) can be computed efficiently in parallel for each $\{u, v\}$, which is useful for handling large-scale MNs. Note that the dual objective is everywhere differentiable while the primal objective is not.

Finally, we can exactly recover the primal solution from the dual solution via (9).

4 Numerical Experiments

In this section, we compare the proposed KLIEP-based method with the graphical-lasso (Glasso) method (Friedman et al., 2008) and the Fused-lasso (Flasso) method (Zhang and Wang, 2010) for Gaussian models, nonparanormal models, and non-Gaussian models (computed with importance sampling). Results are reported on datasets with three different underlying distributions: multivariate Gaussian, nonparanormal, and a non-Gaussian “diamond” distribution. Finally, we show the comparison of the computation time between primal and dual formulations with respect to the input dimensionality. The MATLAB implementation of the proposed method is available at

“<http://sugiyama-www.cs.titech.ac.jp/~song/SCD.html>”.

4.1 Setup

Performance Metrics: By taking advantage of knowing the ground truth of structural changes in artificial experiments, we measure the performance of change detection methods using the *precision-recall (P-R) curve*. For KLIEP and Flasso, a precision and recall curve can be plotted by varying the group-sparsity control parameter λ_2 ; we fix $\lambda_1 = 0$. For Glasso, we vary the sparsity control parameters as $\lambda = \lambda^P = \lambda^Q$.

Model Selection: For KLIEP, we use the log-likelihood of an estimated density ratio on a hold-out dataset, which we refer to as the *hold-out log-likelihood (HOLL)*. More precisely, given two sets of hold-out data $\{\tilde{\mathbf{x}}_i^P\}_{i=1}^{\tilde{n}_P} \stackrel{\text{i.i.d.}}{\sim} P$, $\{\tilde{\mathbf{x}}_i^Q\}_{i=1}^{\tilde{n}_Q} \stackrel{\text{i.i.d.}}{\sim} Q$ for $\tilde{n}_P = \tilde{n}_Q = 3000$, we perform model selection so that the following quantity is maximized:

$$\ell_{\text{HOLL}} = \frac{1}{\tilde{n}_P} \sum_{i=1}^{\tilde{n}_P} \log \frac{\exp \left(\sum_{u \geq v} \hat{\boldsymbol{\theta}}_{u,v}^\top \mathbf{f}(\tilde{\mathbf{x}}_i^{(u)P}, \tilde{\mathbf{x}}_i^{(v)P}) \right)}{\frac{1}{\tilde{n}_Q} \sum_{j=1}^{\tilde{n}_Q} \exp \left(\sum_{u' \geq v'} \hat{\boldsymbol{\theta}}_{u',v'}^\top \mathbf{f}(\tilde{\mathbf{x}}_j^{(u')Q}, \tilde{\mathbf{x}}_j^{(v')Q}) \right)}.$$

When such a hold-out dataset is not available (which happens in real-world experiments shown in the next section), the *cross-validated log-likelihood (CVLL)* is used instead.

For the Glasso, IS-Glasso, and IS-Flasso methods, we perform model selection by maximizing the sum of hold-out/cross-validated log-likelihoods for $p(\mathbf{x}; \boldsymbol{\theta})$ and $q(\mathbf{x}; \boldsymbol{\theta})$:

$$\frac{1}{\tilde{n}_P} \sum_{i=1}^{\tilde{n}_P} \log p(\tilde{\mathbf{x}}_i^P; \hat{\boldsymbol{\theta}}^P) + \frac{1}{\tilde{n}_Q} \sum_{i=1}^{\tilde{n}_Q} \log q(\tilde{\mathbf{x}}_i^Q; \hat{\boldsymbol{\theta}}^Q).$$

For the Flasso method, we maximize the sum of hold-out/cross-validated feature-wise conditional log-likelihood for $p(x^{(s)}|\mathbf{x}^{(-s)}; \boldsymbol{\theta}_s)$ and $q(x^{(s)}|\mathbf{x}^{(-s)}; \boldsymbol{\theta}_s)$ of all nodes:

$$\frac{1}{\tilde{n}_P} \sum_{i=1}^{\tilde{n}_P} \sum_{s=1}^d \log p(\tilde{x}_i^{(s)P} | \tilde{\mathbf{x}}_i^{(-s)P}; \hat{\boldsymbol{\theta}}_s^P) + \frac{1}{\tilde{n}_Q} \sum_{i=1}^{\tilde{n}_Q} \sum_{s=1}^d \log q(\tilde{x}_i^{(s)Q} | \tilde{\mathbf{x}}_i^{(-s)Q}; \hat{\boldsymbol{\theta}}_s^Q).$$

212 **Basis Functions:** We consider two types of \mathbf{f} : a power nonparanormal \mathbf{f}_{npn} and a
 213 polynomial transform \mathbf{f}_{poly} .

The pairwise nonparanormal transform with power k is defined as

$$\mathbf{f}_{\text{npn}}(x_i, x_j) := [\text{sign}(x_i)|x_i|^k \text{sign}(x_j)|x_j|^k, 1].$$

214 This transforms the original data by the power of k , so that the transformed data are
 215 jointly Gaussian (see Section 4.3).

The bivariate polynomial transform up to degree k is defined as

$$\mathbf{f}_{\text{poly}}(x_i, x_j) := [x_i^k, x_j^k, x_i x_j^{k-1}, \dots, x_i^{k-1} x_j, x_i^{k-1}, x_j^{k-1}, \dots, x_i, x_j, 1], \text{ if } i \neq j.$$

216 The univariate polynomial transform is defined as $\mathbf{f}_{\text{poly}}(x_i, x_i) := \mathbf{f}_{\text{poly}}(x_i, 0)$.

217 4.2 Multivariate Gaussian

218 First, we investigate the performance of each learning method under Gaussianity.

Consider a 40-node sparse Gaussian MN, where its graphical structure is characterized by precision matrix $\boldsymbol{\Theta}^P$ with diagonal elements equal to 2. The off-diagonal elements are randomly chosen⁵ and set to 0.2, so that the overall sparsity of $\boldsymbol{\Theta}^P$ is 25%. We then introduce changes by randomly picking 15 edges and reducing the corresponding elements in the precision matrix by 0.1. The resulting precision matrices $\boldsymbol{\Theta}^P$ and $\boldsymbol{\Theta}^Q$ are used for drawing samples as

$$\{\mathbf{x}_i^P\}_{i=1}^n \stackrel{\text{i.i.d.}}{\sim} \mathcal{N}(\mathbf{0}, (\boldsymbol{\Theta}^P)^{-1}) \text{ and } \{\mathbf{x}_i^Q\}_{i=1}^n \stackrel{\text{i.i.d.}}{\sim} \mathcal{N}(\mathbf{0}, (\boldsymbol{\Theta}^Q)^{-1}),$$

219 where $\mathcal{N}(\boldsymbol{\mu}, \boldsymbol{\Sigma})$ denotes the normal distribution with mean $\boldsymbol{\mu}$ and covariance matrix $\boldsymbol{\Sigma}$.
 220 Datasets of size $n = 50$ and $n = 100$ are tested.

221 We repeat the experiments 20 times with randomly generated datasets and report
 222 the results in Figure 3. The top 6 graphs are examples of regularization paths⁶. The
 223 dashed lines represent changed edges in the ground truth while the solid lines represent
 224 unchanged edges. The bottom 3 graphs are the data generating distribution and averaged
 225 P-R curves with standard error. The top row is for $n = 100$ while the middle row is for
 226 $n = 50$. The regularization parameters picked by the model selection procedures described
 227 in Section 4.1 are marked with solid vertical lines. In this experiment, the Gaussian

⁵We set $\Theta_{u,v} = \Theta_{v,u}$ for not breaking the symmetry of the precision matrix.

⁶For all regularization paths plotted in this paper, the paths of univariate factors are removed for clarity.

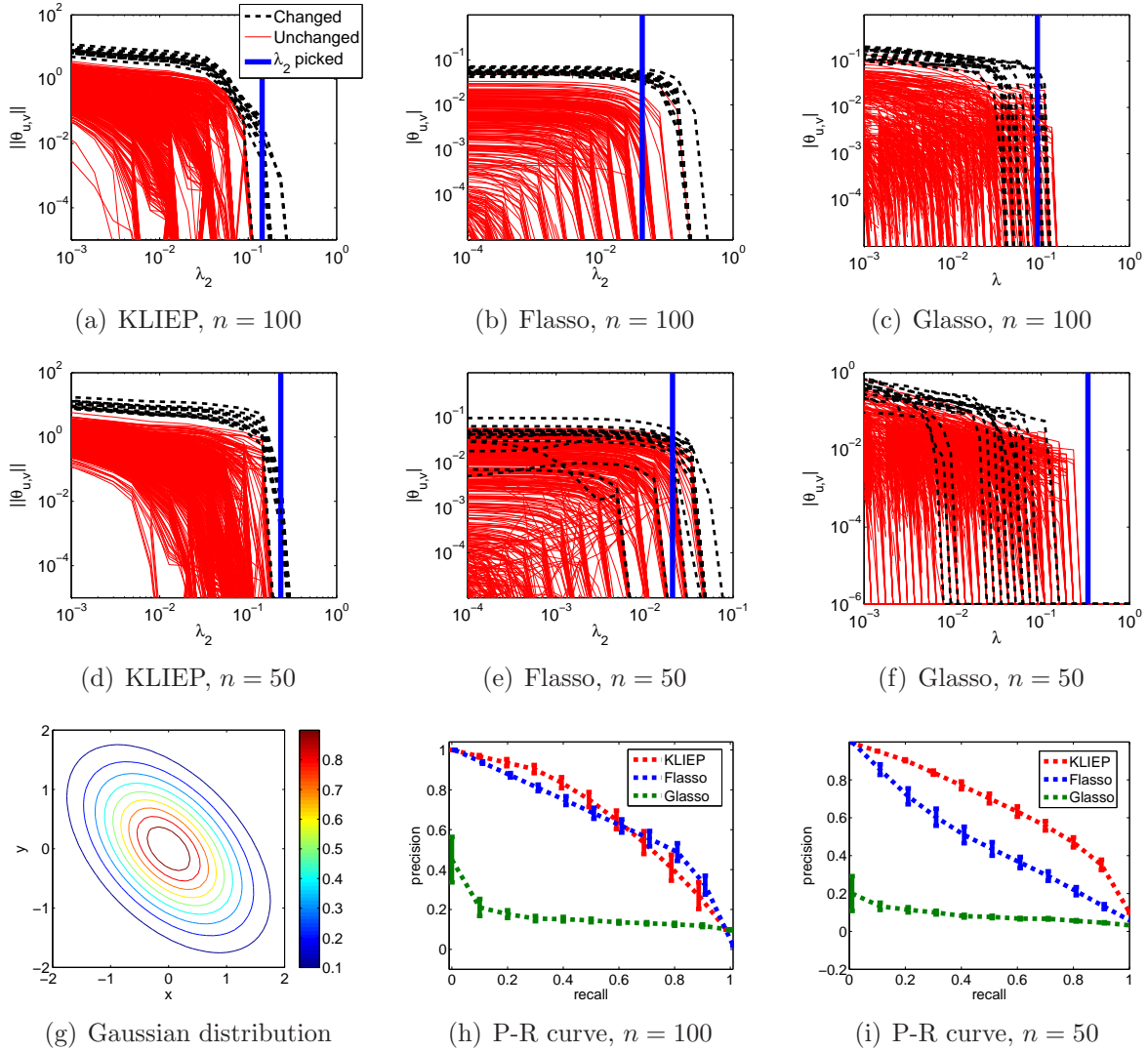


Figure 3: Experimental results on the multivariate Gaussian dataset.

228 model (the nonparanormal basis function with power $k = 1$) is used for KLIEP. Because
 229 the Gaussian model is also assumed in the Flasso and Glasso methods, the difference in
 230 performance is caused only by the difference of estimation methods.

231 When $n = 100$, KLIEP and Flasso clearly distinguish changed (dashed lines) and
 232 unchanged (solid lines) edges in terms of parameter magnitude. However, when the
 233 sample size is halved, the separation is visually rather unclear in the case of Flasso. In
 234 contrast, the paths of changed and unchanged edges are still almost disjoint in the case
 235 of KLIEP. The Glasso method performs rather poorly in both cases. A similar tendency
 236 can be observed also in the averaged P-R curve. When the sample size is 100, KLIEP
 237 and Flasso work equally well, but KLIEP gains its lead when the sample size is reduced.
 238 Glasso does not perform well in both cases.

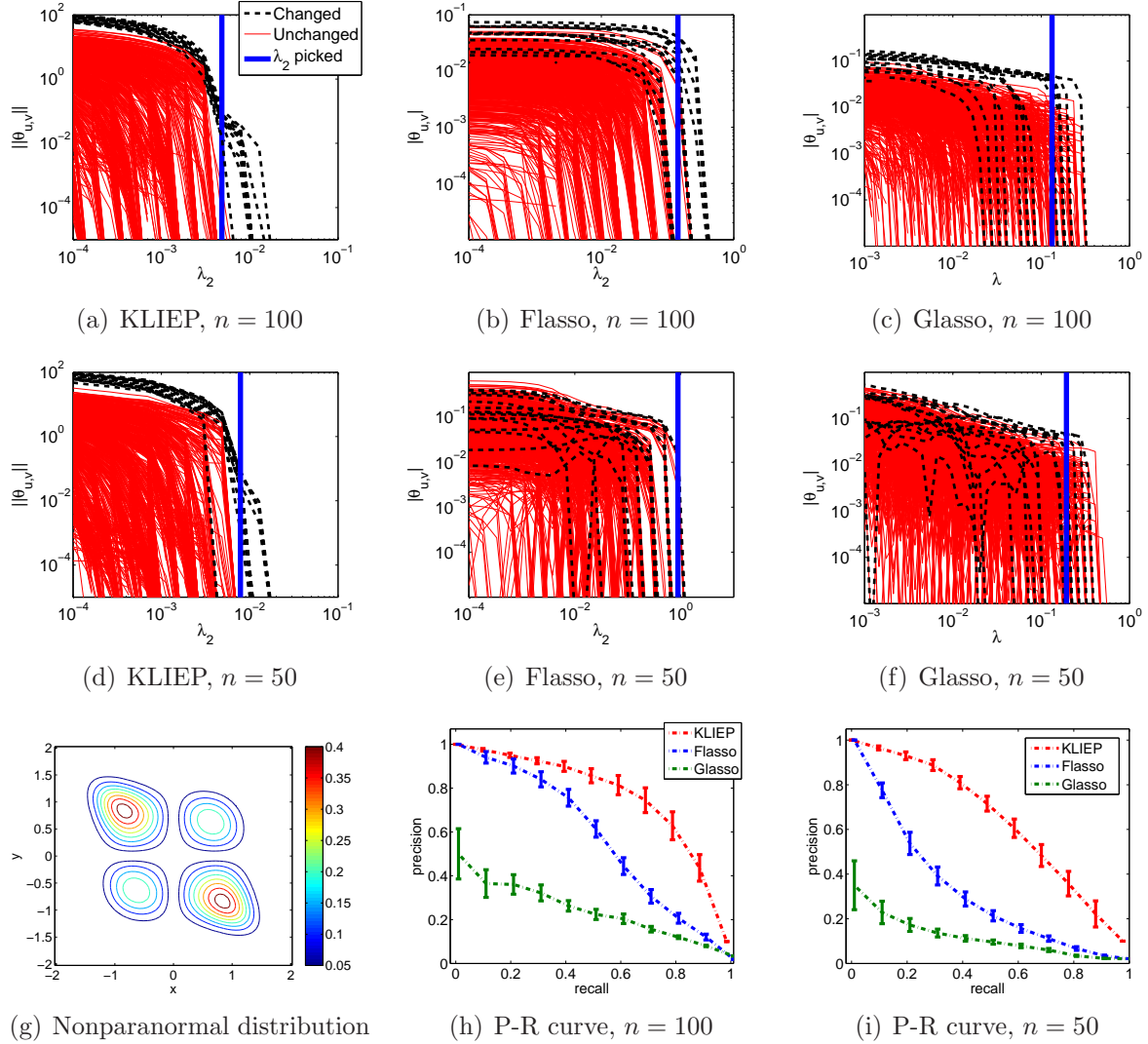


Figure 4: Experimental results on the nonparanormal dataset.

239 4.3 Nonparanormal

We post-process the dataset used in Section 4.2 to construct nonparanormal samples: simply, we apply the power function,

$$h_i^{-1}(x) = \text{sign}(x)|x|^{\frac{1}{2}},$$

240 to each dimension of \mathbf{x}^P and \mathbf{x}^Q , so that $\mathbf{h}(\mathbf{x}^P) \sim \mathcal{N}(\mathbf{0}, (\Theta^P)^{-1})$ and $\mathbf{h}(\mathbf{x}^Q) \sim$
 241 $\mathcal{N}(\mathbf{0}, (\Theta^Q)^{-1})$.

242 In order to cope with the non-linearity, we apply the nonparanormal basis functions
 243 with power $k = 2, 3$, and 4 in KLIEP. Model selection of k is performed in the following
 244 way: for each dataset, the HOLL curve is computed together with the regularization path.
 245 The maximal value among a HOLL curve is referred to as the *peak HOLL*. We select k

that maximizes the peak HOLL on each dataset.

For Flasso and Glasso, we apply the nonparanormal transform described in Liu et al. (2009) before the structural change is learned.

The experiments are conducted on 20 randomly generated datasets with $n = 50$ and 100, respectively. The regularization paths, data generating distribution, and averaged P-R curves are plotted in Figure 4. The results show that Flasso clearly suffers from the performance degradation compared with the Gaussian case, perhaps because the number of samples is too small for the complicated nonparanormal distribution. Due to the two-step estimation scheme, the performance of Glasso is poor. In contrast, KLIEP separates changed and unchanged edges still clearly for both $n = 50$ and $n = 100$. The P-R curves also show the same tendency.

4.4 “Diamond” Distribution with No Pearson Correlation

In the previous experiment, though samples are non-Gaussian, the *Pearson correlation* is not zero. Therefore, methods assuming Gaussianity can still capture the linear correlation between random variables. In this experiment, we consider a more challenging case with a diamond-shaped distribution within the exponential family that has zero Pearson correlation coefficient between variables. Thus, the methods assuming Gaussianity (i.e., Glasso and Flasso) cannot extract any information in principle from this dataset.

The probability density function of the diamond distribution is defined as follows (Figure 5(a)):

$$p(\mathbf{x}) \propto \exp \left(- \sum_{i=1}^d 2x_i^2 - \sum_{(i,j):A_{i,j} \neq 0} 20x_i^2 x_j^2 \right), \quad (11)$$

where the adjacency matrix \mathbf{A} describes the MN structure. Note that this distribution cannot be transformed into a Gaussian distribution by any nonparanormal transformations. Samples from the above distribution are drawn by using a *slice sampling* method (Neal, 2003). However, since generating samples from a high-dimensional distribution is non-trivial and time-consuming, we focus on a relatively low-dimensional case to avoid sampling errors which may mislead the experimental evaluation.

We set $d = 9$ and $n_P = n_Q = 5000$. \mathbf{A}^P is randomly generated with 35% sparsity, while \mathbf{A}^Q is created by randomly removing edges in \mathbf{A}^P so that the sparsity level is dropped to 15%.

In this experiment, we compare the performance of all methods with their available transforms: KLIEP ($\mathbf{f}_{\text{poly}}, k = 2, 3, 4$), KLIEP ($\mathbf{f}_{\text{npn}}, k = 2, 3, 4$), KLIEP (Gaussian; equivalent to \mathbf{f}_{npn} with $k = 1$), Flasso (nonparanormal), Flasso (Gaussian), Glasso (nonparanormal) and Glasso (Gaussian). For comparing with the sampling-based non-Gaussian MLE, we also include IS-Glasso ($\mathbf{f}_{\text{poly}}, k = 4$; the correct model) and IS-Flasso ($\mathbf{f}_{\text{poly}}, k = 4$) in the comparison. We set the instrumental distribution p' as $\mathcal{N}(\mathbf{0}, \mathbf{I})$, and use sample $\{\mathbf{x}\}_{i=1}^{70000} \sim p'$ for approximating integrals using importance sampling.

280 p' is purposely chosen so it has a similar “bell” shape but with larger variance on each
 281 dimension comparing to p or q .

282 The averaged P-R curves over 20 datasets are shown in Figure 5(e). KLIEP (\mathbf{f}_{poly}) sig-
 283 nificantly outperforms all the other methods, while the IS-Glasso and especially IS-Flasso
 284 give better result than KLIEP (Gaussian and NPN), Flasso- and Glasso-based methods.
 285 This means that the polynomial kernel is indeed very helpful in handling completely non-
 286 Gaussian data. However, as discussed in Section 2.2, it is difficult to use such a kernel in
 287 Glasso and Flasso because of the computational intractability of the normalization term.
 288 Although IS-Glasso can approximate integrals, the result shows that such approximation
 289 of integrals does not lead to a very good performance. In comparison, the result of IS-
 290 Flasso method is much improved thanks to the coupled sparsity regularization, but it is
 291 still not comparable to KLIEP.

292 The regularization path of KLIEP (\mathbf{f}_{poly}) illustrated in Figure 5(b) shows the useful-
 293 ness of the proposed method in change detection under non-Gaussianity. We also give
 294 regularization paths obtained by IS-Glasso and IS-Flasso methods on the same dataset
 295 on Figures 5(c) and 5(d). It can be seen that both paths do not fit the ground truth well,
 296 though the IS-Flasso method works slightly better.

297 4.5 Computation Time: Dual versus Primal Optimization Prob- 298 lems

299 Finally, we compare the computation time for solving the dual optimization problem
 300 (10) and the primal optimization problem (6). Both optimizations are carried out by
 301 using the same convex solver *minFunc*⁷. The datasets are generated from two Gaussian
 302 distributions constructed in the same way as that is described in Section 4.2. 150 samples
 303 are separately drawn from two distributions with dimension $d = 40, 50, 60, 70, 80$. We
 304 then perform the structural change detection by computing the entire regularization path
 305 using 20 choices of λ_2 ranging from 10^{-4} to 10^0 and fix $\lambda_1 = 0.1$. The results are plotted
 306 in Figure 6.

307 It can be seen from the graph that as the dimensionality increases, the computation
 308 time for solving the primal optimization problem is sharply increased, while that for
 309 solving the dual optimization problem grows only moderately. It is noteworthy that when
 310 $d = 80$, the computation time for obtaining the primal solution is almost 10 times more
 311 than that required for obtaining the dual solution.

312 5 Applications

313 In this section, experiments are conducted on a synthetic gene expression dataset and on
 314 a Twitter dataset, respectively. For both experiments, we consider KLIEP and Flasso
 315 methods, while for the gene expression dataset, the variant of Flasso, IS-Flasso is also
 316 included. For KLIEP and IS-Flasso, the polynomial transform function with $k \in \{2, 3, 4\}$

⁷<http://www.di.ens.fr/~mschmidt/Software/minFunc.html>

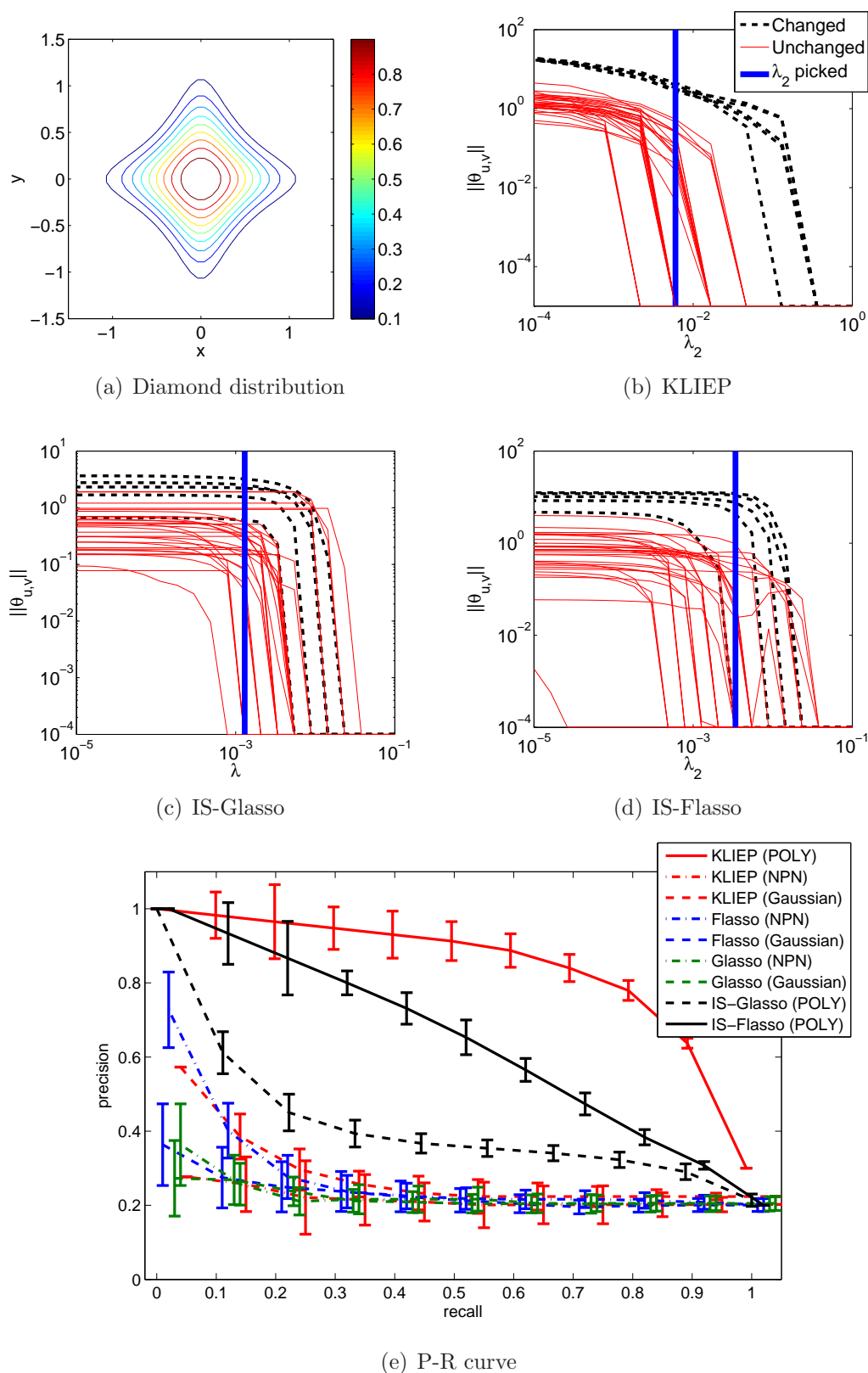


Figure 5: Experimental results on the diamond dataset. “NPN” and “POLY” denote the nonparanormal and polynomial models, respectively. Note that the precision rate of 100% recall for a random guess is approximately 20%.

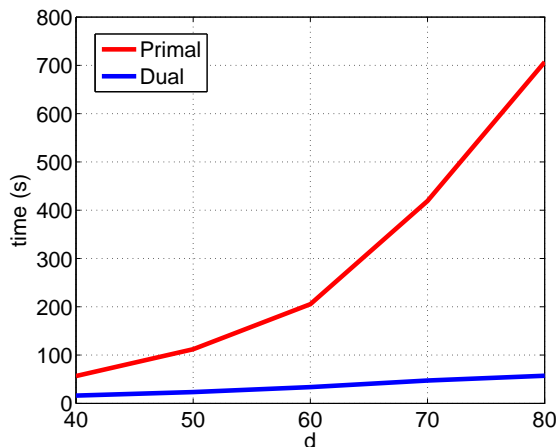


Figure 6: Comparison of computation time for solving primal and dual optimization problems.

317 is used. The parameter λ_1 in KLIEP and Flasso is tested with choices $\lambda_1 \in \{0.1, 1, 10\}$.
 318 The performance reported for the experiments in Section 5.1 and Section 5.2 are obtained
 319 using the models selected by HOLL and 5-fold CVLL (see Section 4.1), respectively.

320 5.1 Synthetic Gene Expression Dataset

321 A gene regulatory network encodes interactions between DNA segments. However, the
 322 way genes interact may change due to environmental or biological stimuli. In this exper-
 323 iment, we focus on detecting such changes. We use *SynTReN*, which is a generator of
 324 gene regulatory networks used as the benchmark validation of bioinformatics algorithms
 325 (Van den Bulcke et al., 2006).

326 To test the applicability of the proposed method, we first choose a sub-network con-
 327 taining 13 nodes from an existing signaling network in *Saccharomyces cerevisiae* (shown
 328 in Figure 7(a)). Three types of interactions are modeled: activation (ac), deactivation
 329 (re), and dual (du). 50 samples are generated in the first stage, after which we change the
 330 types of interactions in 6 edges, and generate 50 samples again. Four types of changes
 331 are considered in such case: $ac \rightarrow re$, $re \rightarrow ac$, $du \rightarrow ac$, and $du \rightarrow re$.

332 We set the instrumental distribution p' as $\mathcal{N}(\mathbf{0}, \mathbf{I})$, and use sample $\{\mathbf{x}\}_{i=1}^{70000} \sim p'$ for
 333 approximating integrals using importance sampling.

334 The regularization paths on one example dataset for KLIEP, Flasso and IS-Flasso are
 335 plotted in Figures 7(b), 7(c) and 7(d). Averaged P-R curves over 20 simulation runs are
 336 shown in Figure 7(e). Clearly from the example of KLIEP regularization paths shown in
 337 Figure 7(b), the magnitude of estimated parameters on the changed pairwise interactions
 338 is much higher than that of the unchanged ones, and hits zero only at the final stage.
 339 On the other hand, Flasso gives many false alarms by assigning non-zero parameters
 340 to the unchanged interactions, even after some changed ones hit zeros. However, IS-

341 Flasso illustrates much clearer separation between changed and unchanged interactions
 342 on Figure 7(d) though there are still a few unchanged interactions drop to zero at the
 343 final stage.

344 Reflecting a similar pattern, the P-R curves plotted in Figure 7(e) show that the
 345 proposed KLIEP method has the best performance among all three methods, although
 346 the IS-Flasso method has achieved significant improvement over Flasso method. The
 347 improvement from Flasso to IS-Flasso shows that the polynomial kernel does improve the
 348 performance on this dataset, while the improvement from IS-Flasso to KLIEP shows that
 349 the direct estimation can further boost the performance.

350 5.2 Twitter Story Telling

351 In this experiment, we use KLIEP and Flasso as event detectors from Twitter. More
 352 specifically, we choose the *Deepwater Horizon oil spill*⁸ as the target event, and we hope
 353 that our method can recover some story lines from Twitter as the news event develops.
 354 Counting the frequencies of 10 keywords (BP, oil, spill, Mexico, gulf, coast, Hayward,
 355 Halliburton, Transocean, and Obama), we obtain a dataset by sampling 1061 times (4
 356 per day), from February 1st, 2010 to October 15th, 2010.

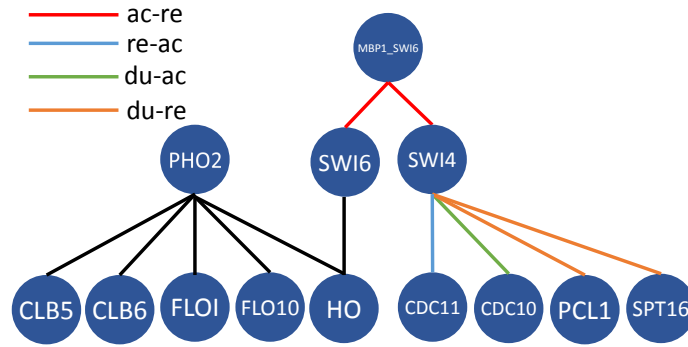
357 To conduct our experiments, we segment the data into two parts. The first 300 samples
 358 collected before the day of oil spill (April 20th, 2010) are regarded as conforming to a
 359 10-dimensional joint distribution Q , while the second set of samples that are drawn in an
 360 arbitrary 50-day window approximately after the event happened is regarded as following
 361 distribution P .

362 The MN of Q encodes the original conditional independence of frequencies between
 363 10 keywords, and the underlying MN of P has changed since an event occurred. Thus,
 364 unveiling changes in MNs between P and Q may recover popular topic trends on Twitter
 365 in terms of the dependency among keywords.

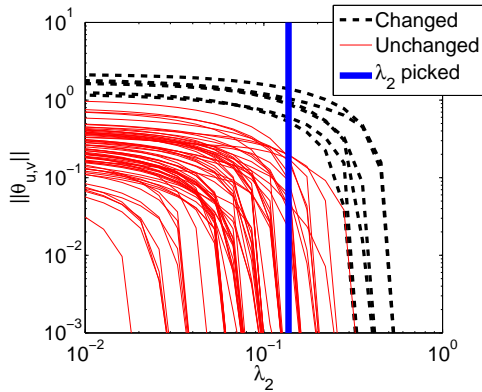
366 The detected change graphs (i.e., the graphs with only detected changing edges) on
 367 10 keywords are illustrated in Figure 8. The edges are selected at a certain value of λ_2
 368 indicated by the maximal CVLL. Since the edge set that is picked by CVLL may not
 369 be sparse in general, we sparsify the graph based on the permutation test as follows:
 370 we randomly shuffle the samples between P and Q and repeatedly run change detection
 371 algorithms for 100 times; then we observe detected edges by CVLL. Finally, we select
 372 the edges that are detected using the original non-shuffled dataset and remove those that
 373 were detected in the shuffled datasets for more than 5 times. In Figure 8, we plot detected
 374 change graphs which are generated using samples of P starting from April 17th, July 6th,
 375 and July 26th.

376 The initial explosion happened on April 20th, 2010. Both methods discover depen-
 377 dency changes between keywords. Generally speaking, KLIEP captures more conditional
 378 independence changes between keywords than the Flasso method, especially when com-
 379 paring Figure 8(c) and Figure 8(f). At the first two stages (Figure 8(a),8(d), 8(b) and

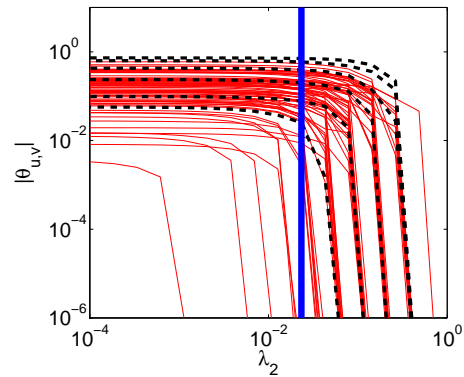
⁸http://en.wikipedia.org/wiki/Deepwater_Horizon_oil_spill



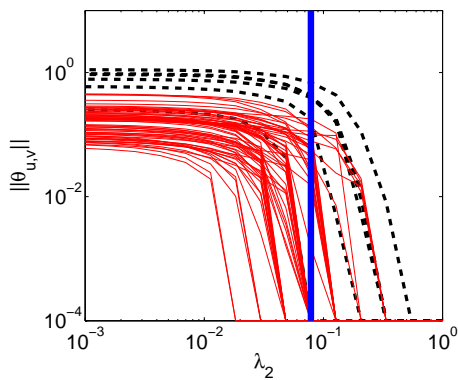
(a) Gene regulatory network



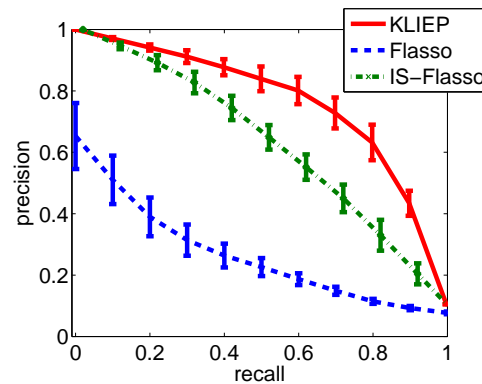
(b) KLIEP



(c) Flasso

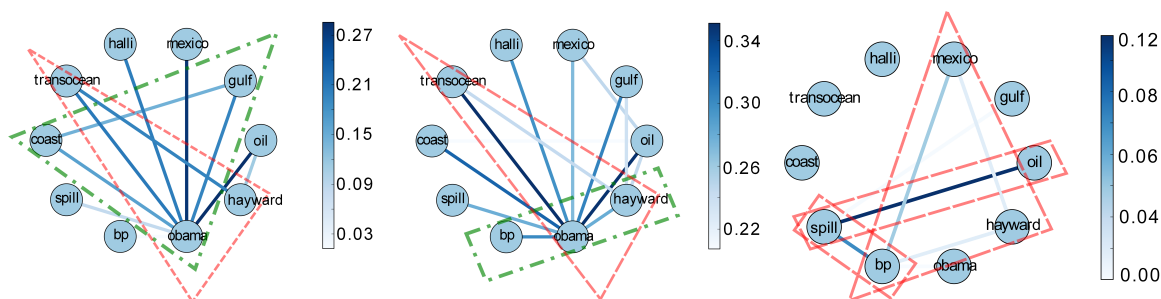


(d) IS-Flasso

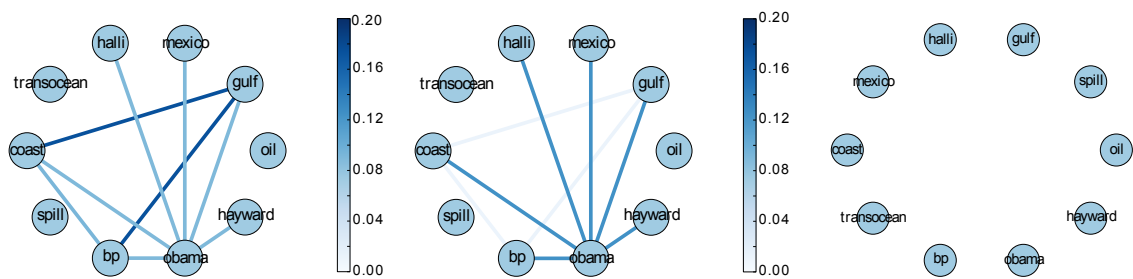


(e) P-R curve

Figure 7: Experiments on synthetic gene expression datasets.



(a) April 17th–June 5th, KLIEP (b) June 6th–July 25th, KLIEP (c) July 26th–Sept. 14th, KLIEP



(d) April 17th–June 5th, Flasso (e) June 6th–July 25th, Flasso (f) July 26th–Sept. 14th, Flasso

Figure 8: Change graphs captured by the proposed KLIEP method (top) and the Flasso method (bottom). The date range beneath each figure indicates when P was sampled, while Q is fixed to dates from February 1st to April 20th. Notable structures shared by the graph of both methods are surrounded by the dash-dotted lines. Unique structures that only appear in the graph of the proposed KLIEP method are surrounded by the dashed lines.

380 8(e)), the keyword “Obama” is very well connected with other keywords
 381 given by both methods. Indeed, at the early development of this event, he lies in the
 382 center of the news stories, and his media exposure peaks after his visit to the Louisiana
 383 coast (May 2nd, May 28nd, and June 5th) and his meeting with BP CEO Tony Hay-
 384 ward on June 16th. Notably, both methods highlight the “gulf-obama-coast” triangle
 385 in Figure 8(a) and Figure 8(d) and the “bp-obama-hayward” chain in Figure 8(b) and
 386 Figure 8(e).

387 However, there are some important differences worth mentioning. First, the Flasso
 388 method misses the “transocean-hayward-obama” triangle in Figure 8(d) and Figure 8(e).
 389 Transocean is the contracted operator in the Deepwater Horizon platform, where the
 390 initial explosion happened. On Figure 8(c), the chain “bp-spill-oil” may indicate that the
 391 phrase “bp spill” or “oil spill” has been publicly recognized by the Twitter community
 392 since then, while the “hayward-bp-mexico” triangle, although relatively weak, may link
 393 to the event that Hayward stepped down from the CEO position on July 27th.

6 Conclusion and Future Work

In this paper, we proposed a *direct* approach to learning sparse changes in MNs by density ratio estimation. Rather than fitting two MNs separately to data and comparing them to detect a change, we estimated the ratio of the probability densities of two MNs where changes can be naturally encoded as sparsity patterns in estimated parameters. Through experiments on artificial and real-world datasets, we demonstrated the usefulness of the proposed method.

Compared with the conventional two-stage MLE approach, a notable advantage of our method is that the normalization term in the density ratio model can be approximated by a sample average without sampling. This considerably loosens the restriction on applicable distributions. Our experiment also showed that even when the sampling-based method is included, the proposed method still outperformed all state-of-the-art methods on non-Gaussian data. Moreover, thanks to its direct modeling nature with density ratios, the number of parameters is halved. With the dual formulation derived in this paper, the number of parameters can be even further reduced, which is highly useful when the dimensionality is high.

We only considered MNs with pairwise factors in this paper. However, such a model may be misspecified when higher order interactions exist. For example, combination with the idea of *hierarchical log-linear models* presented in Schmidt and Murphy (2010) may lead to a promising solution to this problem, which will be investigated in our future work.

Acknowledgement

SL is supported by the JST PRESTO program and the JSPS fellowship, JQ is supported by the JST PRESTO program, and MS is supported by the JST CREST program. MUG is supported by the Finnish Centre-of-Excellence in Computational Inference Research COIN (251170). TS was partially supported by MEXT Kakenhi 25730013, and the Aihara Project, the FIRST program from JSPS, initiated by CSTP.

References

- O. Banerjee, L. El Ghaoui, and A. d’Aspremont. Model selection through sparse maximum likelihood estimation for multivariate Gaussian or binary data. *Journal of Machine Learning Research*, 9:485–516, March 2008.
- C. M. Bishop. *Pattern Recognition and Machine Learning*. Springer, New York, NY, USA, 2006.
- S. Boyd and L. Vandenberghe. *Convex Optimization*. Cambridge University Press, Cambridge, UK, 2004.

- 428 J. Friedman, T. Hastie, and R. Tibshirani. Sparse inverse covariance estimation with the
429 graphical lasso. *Biostatistics*, 9(3):432–441, 2008.
- 430 A. Gelman. Method of moments using Monte Carlo simulation. *Journal of Computational
431 and Graphical Statistics*, 4(1):36–54, 1995.
- 432 M. U. Gutmann and A. Hyvärinen. Noise-contrastive estimation of unnormalized statisti-
433 cal models, with applications to natural image statistics. *Journal of Machine Learning
434 Research*, 13:307–361, 2012.
- 435 T. Hastie, R. Tibshirani, and J. Friedman. *The Elements of Statistical Learning: Data
436 Mining, Inference, and Prediction*. Springer, New York, NY, USA, 2001.
- 437 G. E. Hinton. Training products of experts by minimizing contrastive divergence. *Neural
438 computation*, 14(8):1771–1800, 2002.
- 439 A. Hyvärinen. Estimation of non-normalized statistical models by score matching. In
440 *Journal of Machine Learning Research*, volume 6, pages 695–709, 2005.
- 441 D. Koller and N. Friedman. *Probabilistic Graphical Models: Principles and Techniques*.
442 MIT press, 2009.
- 443 S.-I. Lee, V. Ganapathi, and D. Koller. Efficient structure learning of Markov networks
444 using l_1 -regularization. In B. Schölkopf, J. Platt, and T. Hoffman, editors, *Advances
445 in Neural Information Processing Systems 19*, pages 817–824, Cambridge, MA, 2007.
446 MIT Press.
- 447 H. Liu, J. Lafferty, and L. Wasserman. The nonparanormal: Semiparametric estimation
448 of high dimensional undirected graphs. *The Journal of Machine Learning Research*, 10:
449 2295–2328, 2009.
- 450 H. Liu, F. Han, M. Yuan, J. Lafferty, and L. Wasserman. The nonparanormal skeptic. In
451 *Proceedings of the 29th International Conference on Machine Learning (ICML2012)*,
452 2012.
- 453 N. Meinshausen and P. Bühlmann. High-dimensional graphs and variable selection with
454 the lasso. *The Annals of Statistics*, 34(3):1436–1462, 2006.
- 455 R. M Neal. Slice sampling. *The Annals of Statistics*, 31(3):705–741, 2003.
- 456 P. Ravikumar, M. J. Wainwright, and J. D. Lafferty. High-dimensional Ising model selec-
457 tion using l_1 -regularized logistic regression. *The Annals of Statistics*, 38(3):1287–1319,
458 2010.
- 459 C. P. Robert and G. Casella. *Monte Carlo Statistical Methods*. Springer-Verlag New York,
460 Inc., Secaucus, NJ, USA, 2005.

- 461 M. W. Schmidt and K. P. Murphy. Convex structure learning in log-linear models: Beyond
462 pairwise potentials. *Journal of Machine Learning Research - Proceedings Track*, 9:709–
463 716, 2010.
- 464 M. Sugiyama, T. Suzuki, S. Nakajima, H. Kashima, P. von Bünau, and M. Kawanabe.
465 Direct importance estimation for covariate shift adaptation. *Annals of the Institute of*
466 *Statistical Mathematics*, 60(4):699–746, 2008.
- 467 M. Sugiyama, T. Suzuki, and T. Kanamori. *Density Ratio Estimation in Machine Learn-*
468 *ing*. Cambridge University Press, Cambridge, UK, 2012.
- 469 R. Tibshirani, M. Saunders, S. Rosset, J. Zhu, and K. Knight. Sparsity and smooth-
470 ness via the fused lasso. *Journal of the Royal Statistical Society: Series B (Statistical*
471 *Methodology)*, 67(1):91–108, 2005.
- 472 Y. Tsuboi, H. Kashima, S. Hido, S. Bickel, and M. Sugiyama. Direct density ratio es-
473 timation for large-scale covariate shift adaptation. *Journal of Information Processing*,
474 17:138–155, 2009.
- 475 T. Van den Bulcke, K. Van Leemput, B. Naudts, P. van Remortel, H. Ma, A. Verschoren,
476 B. De Moor, and K. Marchal. SynTReN: A generator of synthetic gene expression data
477 for design and analysis of structure learning algorithms. *BMC Bioinformatics*, 7(1):43,
478 2006.
- 479 V. N. Vapnik. *Statistical Learning Theory*. Wiley, New York, NY, USA, 1998.
- 480 M. J. Wainwright and M. I. Jordan. Graphical models, exponential families, and varia-
481 tional inference. *Foundations and Trends® in Machine Learning*, 1(1-2):1–305, 2008.
- 482 L. Wasserman. *All of Statistics: A Concise Course in Statistical Inference*. Springer
483 Publishing Company, Incorporated, 2010.
- 484 B. Zhang and Y.J. Wang. Learning structural changes of Gaussian graphical models in
485 controlled experiments. In *Proceedings of the Twenty-Sixth Conference on Uncertainty*
486 *in Artificial Intelligence (UAI2010)*, pages 701–708, 2010.
- 487 H. Zou and T. Hastie. Regularization and variable selection via the elastic net. *Journal*
488 *of the Royal Statistical Society, Series B*, 67(2):301–320, 2005.